I&EC research
Industrial & Engineering Chemistry Research

Separations

Influence of iron additive on the hydrogen separation properties of carbon molecular sieve membranes

Izumi Kumakiri, Kyosuke TAMURA, Yukichi Sasaki, Kazuhiro Tanaka, and Hidetoshi Kita

Ind. Eng. Chem. Res., **Just Accepted Manuscript** • DOI: 10.1021/acs.iecr.7b05265 • Publication Date (Web): 16 Mar 2018

Just Accepted

ACS Publications

is published by the American Chemical Society. 1155 Sixteenth Street N.W., Washington, DC 20036

Influence of iron additive on the hydrogen separation properties of carbon molecular sieve membranes

I. Kumakiri [a,*], K. Tamura [a], Y. Sasaki [b], K. Tanaka [a] and H. Kita [a]

a: Yamaguchi University, Graduate School of Sciences and Technology for Innovation, 2-16-1 Tokiwadai Ube Yamaguchi, 755-8611 Japan

b: Japan Fine Ceramics Center, JFCC, 2-4-1 Mutsuno,Atsuta-ku,Nagoya,456-8587 Japan

* Corresponding author: e-mail: izumi.k@yamaguchi-u.ac.jp

Abstract

Carbon molecular sieve (CMS) membranes were prepared on the outer surface of porous ceramic tubes using a lignin-based material, organosolve-lignin, and a phenol resin, Bellpeal-S899, as precursors. Higher pyrolysis temperature resulted in higher hydrogen selectivity over oxygen or other larger gases, but hydrogen permeance decreased significantly. On the contrary, addition of a small amount of iron(Ⅲ) acetate basic to the precursors improved the hydrogen selectivity but maintained the hydrogen permeance. Addition of iron compound to the precursor strongly reduced the permeances of nitrogen and methane through the resulting CMS membranes. Distribution of iron in the carbon matrix was evaluated by TEM-EDS and EPMA analyses. Aging influence on the membrane permeance was also studied. The results suggest the possibility to tune the size of ultra-micropores in CMS membranes using additives.

Key words

Carbon molecular sieve membrane, Lignin, Phenol resin, Gas separation, Hydrogen

Introduction

The emission of carbon dioxide needs to be reduced to limit the global temperature increase well below 2 degree Celsius as agreed in the Paris agreement [1]. A hydrogen-based economy is considered as an alternative to the fossil fuel-based economy, and significant efforts have been made in developing related technologies[2]. For example, integrating a carbon capture process to steam reforming of hydrocarbons is a way to generate hydrogen with less carbon emission to the atmosphere. Alternatively, hydrogen can be generated by water splitting using renewable energy, by photocatalytic splitting of water, or by other methods. Transport and storage of hydrogen also have various options[2]. One idea is to convert hydrogen to a chemical hydrogen carrier, such as methylcyclohexane (MCH), which is liquid at ambient temperature and pressure[3, 4]. One of the advantages of the MCH system is the possibility of using existing petroleum distribution infrastructures[3, 5]. Handling of liquid MCH is easier compared to dealing with liquid hydrogen, which requires cooling. Therefore, the MCH system is considered as a suitable option for long distance transport and large-scale storage [3, 4].

In the MCH system, hydrogen is generated by a dehydrogenation reaction (MCH → Toluene + $3H_2$) followed by a separation. A demonstration plant with a capacity of 50 Nm^3-H_2/h was constructed in Japan[5]. Besides scaling-up the dehydrogenation plant, performing

dehydrogenation at a fueling station was also considered through the "Energy Carrier Program" funded by the Japan Science and Technology Agency and through other projects[6, 7]. Safety and risk analyses were also performed[7]. One of the technological challenges related to this application is to develop energy-efficient and compact dehydrogenation and separation processes. Large part of the toluene formed after the dehydrogenation can be liquefied and removed by cooling. However, a small amount of toluene, corresponding to its vapor pressure, mixes with the hydrogen. For example, after cooling at 308K and 0.3MPa, a mixture of 2% toluene and 98% hydrogen is obtained [8]. As the carbon content should be less than 2ppm for the use in fuel cell vehicles, further purification process is required. A process simulation suggested that to achieve the hydrogen purity requirement with a hydrogen recovery of 90% in a single separation unit, membranes with hydrogen/toluene selectivity over 280,000 are required [8]. In this case, the consumed energy at the separator was calculated to be 0.12 kWh Nm^{-3}–H_2, which is about half of the energy consumed using conventional pressure swing adsorption that requires 0.26 kWh Nm^{-3}–H_2 [8]. Membranes can be used not only as a separator after the dehydrogenation, but also be applied at the dehydrogenation reaction. Removing hydrogen from the dehydrogenation reaction through a membrane shifts the reaction for higher yield. In addition such membrane reactors can lower the reaction temperature to e.g. 500 K [9-11]. As the size of the hydrogen molecule is much smaller compared to the size of MCH and toluene molecules,

hydrogen can be separated by molecular-sieving. Palladium-alloy membranes show quite high hydrogen selectivity but these membranes require ca. 573K or higher as operating temperature[12]. Therefore, micro-porous membranes, such as micro-porous silica[9-11], zeolites[13] and carbon molecular sieve (CMS) membranes[14], are considered to have high potentials in the MCH system.

CMS membranes show high hydrogen selectivity among various types of micro-porous inorganic membranes. Yoshimune et al. reported that CMS membranes showed hydrogen selectivity over 300,000 (toluene content in the permeate was lower than the detection limit) when hydrogen containing 0.5mol% toluene was fed at 363K[15]. The selectivity and the hydrogen permeance were kept almost constant for over 500 hours. This selectivity satisfies the required selectivity for the separation process after the dehydrogenation[8]. The drawbacks of CMS membranes are their brittleness and rather small permeation flux. For example, hydrogen permeance is often 1-2 orders smaller than the permeance through micro-porous silica membranes[16]. In addition, as the CMS membranes have hydrophobic nature, adsorption of toluene to the CMS membrane is another issue needing further study.

CMS membranes are prepared by pyrolyzing polymeric membranes under inert conditions, There are two major geometries for CMS membranes; hollow fibers [17, 18, 19] and composite membranes on porous supports[14, 20-22]. In the latter case, porous supports are coated with

polymeric films by e.g. dip-coating followed by pyrolysis. As the support gives mechanical strength, CMS membranes can be thin, which is expected to improve the flux. The type of precursors and preparation conditions, such as pyrolysis conditions, affect membrane performances[23, 24]. Membrane properties can be tuned by controlling the sorption and diffusion characteristics. Various methods can be applied[23], such as pre-treating the precursor layers, mixing nano-particles to the precursors[25-28] and post-treatments[29]. For example, Yoda et al. reported that dispersing Pd particles of ca. 5nm increased the hydrogen selectivity of CMS membranes due to their strong affinity to hydrogen [25]. Suda et al.[26] and Chu et al.[28] suggested that Fe(Ⅱ) compound incorporated to the membrane narrow the pore size.

Cellulose derivatives, polyimide and polyacrylonitrile are some common precursors used to prepare CMS membranes [24]. In this study, lignin based material was used to investigate a new type of precursor. Preparation conditions were optimized to form CMS membranes on porous alumina tubes targeting to improve hydrogen permeance. The influence of adding iron compounds to the precursors on the hydrogen permeance and selectivity of resulting CMS membranes was examined. The influence of aging in the air was also studied.

Experimental section

Presursors

A lignin-based material, organosolve-lignin (OrL, Sigma-Aldrich) and a phenol resin (Bellpearl S899, BP, Air Water Bellpearl) were used as precursor. Figure 1 shows the structure of OrL. Both precursors are thermoplastic and self-curing according to the product information[30] and may heal small cracks in the precursor film during the pyrolysis. Precursors were dissolved in tetrahydrofuran (THF). The concentration of a precursor solution affects the CMS membrane formation: too low precursor concentration resulted in non-continuous carbon layer, while too high concentration resulted in thick coating layer that tended to peeling off from the support. After trial and error, the concentration was adjusted to 30wt% in this study. In some cases, iron(Ⅲ) acetate basic ($Fe(OH)(CH_3COO)_2$, FeAc, Kishida Chemical Co. Ltd.) was added to the OrL or BP precursor solution. The amount of iron acetate addition was 1.7 wt% to the amount of precursor. FeAc and dried precursor solutions were analyzed by thermogravimetric analysis (TG, Rigaku, Thermo plus TG 8120) with a heating rate of 5K/min in a nitrogen atmosphere. Dried precursor solutions were pyrolyzed under the same conditions as CMS membranes as described in the following, then analyzed by transmission electron microscope (TEM, JEOL, JEM-2010) and energy dispersive X-ray spectroscopy (EDS, NORAN instruments, VANTAGE).

Membrane preparation

Porous α-alumina tubes (NOK Co. Japan, pore size: 0.1 μm, o.d. 3 mm, length 50 mm)

were used as supports. After washing and drying, supports were immersed in the precursor solution for 10 minutes and then withdrew at a rate of 1 cm/min. Both ends of the supports were sealed with a Teflon tape beforehand the dipping, to apply coating on the outer surface of the support. Membranes were dried at 343K for 8 hours after the dip-coating, and then dried in a vacuum oven at 373K for 24 hours to remove the solvent. Precursor-coated membranes were pyrolyzed at 773 to 973 K by an induction heating unit with a nitrogen flow of 200 mL/min. Temperature program is shown in Figure 2. The ramp rate was controlled to reach the target temperature in 3 minutes. After keeping the pyrolysis temperature for 10 minutes, the heating unit was turned off. The temperature decreased to around 400K in 15 minutes and then the CMS membrane was removed from the oven. A membrane number in the following shows the precursor type and the pyrolysis temperature.

Membrane characterization

Membrane surface and cross-sectional morphologies were characterized by a field emission scanning electron microscopy (FE-SEM, JEOL JSM 6335F). An electron probe micro-analyzer (EPMA, Shimadzu EPMA-1720) was used to examine the thickness of a carbon layer and the distribution of iron. Single gas permeation was measured at 308K by a fixed volume method. Figure 3 shows a schematic drawing of the setup. The membrane was placed in

a stainless-steel module and both ends were sealed with Viton O-rings. One end of the permeate line was closed. Feed gas was introduced to the outer surface of the CMS membrane. The feed pressure was maintained at 1.1 atm. Vacuum was applied at the permeate side. The effective membrane area was about 3.8cm^2. Beforehand the measurements, membranes were heated at 408K for 2 hours under vacuum to remove adsorbed molecules. The ideal selectivity was calculated by the ratio of single-gas permeance of two types of gas.

Results and discussion

CMS membranes prepared from a pure OrL precursor

Figure 4 shows the influence of pyrolysis temperature on the gas permeation properties when membranes were prepared from a pure OrL precursor. Coating and pyrolysis process was repeated twice to eliminate possible defects in the membrane. Pyrolysis temperature had a strong influence on the single gas permeance. For example, hydrogen permeance was 47.8 nmol·m^{-2}·s^{-1}·Pa^{-1} after pyrolyzing at 673K, but increased to 124 nmol·m^{-2}·s^{-1}·Pa^{-1} after pyrolyzing at 773K. Hydrogen permeance then decreased significantly by increasing the pyrolysis temperature to 12 nmol·m^{-2}·s^{-1}·Pa^{-1} and 3.7 nmol·m^{-2}·s^{-1}·Pa^{-1} after pyrolyzing at 873 K and 973 K, respectively. Similar trend was observed with He, CO_2 and O_2. This is a common observation with CMS membranes and explained by the formation of micro-pores that increases

the permeance, and by the shrinkage of micro-pores at higher temperature that decreases the permeance [31]. Permeance of N_2 or other larger molecules decreased with increasing the pyrolysis temperature, suggesting the formation of ultra-micro-pores (pores of approximate size smaller than 0.7 nm[32]) having smaller size than the size of nitrogen molecule by the pyrolysis. The ideal selectivities of hydrogen to methane and hydrogen to oxygen became higher with higher pyrolysis temperature and showed the maximum ideal selectivities of 630 and 29, respectively, after pyrolyzing at 973K as shown in Figure 4 and Table 1. Ideal selectivity of carbon dioxide to nitrogen or methane also increased with pyrolysis temperature and showed the maximum values of 35 for carbon dioxide to nitrogen and 140for carbon dioxide to methane at 873K. After pyrolysis at 1073K, the CMS membrane lost selectivity due to crack formations. Repeating the coating, drying and pyrolysis step did not show strong influence on the hydrogen selectivity when membranes were pyrolyzed at773K as shown in Table 1. The hydrogen permeance was smaller after repeating the coating-pyrolysis step twice, due to the increase in the membrane thickness. As the target of this study was to improve the hydrogen permeance, pyrolysis temperature of 773 K, at which temperature the highest hydrogen permeance was obtained, was used in the following experiments.

Influence of iron compound in the precursor

Iron(Ⅲ) acetate basic totally decomposed by 600K as reported earlier [33]. Figure 5 shows the TG of the precursors. The weight loss at 773K was about 60% and 35% for OrL and BP, respectively. Addition of 1.7 wt% iron compounds to the precursor solutions slightly decreased the decomposition temperature for both OrL and BP precursors.

After a single step of coating followed by pyrolysis at 773K, a CMS layer of ca. 1 micromater thickness was formed on the porous support as shown in Figure 6a. EPMA showed the carbon layer was mainly formed on the support surface (Figure 6b). Iron was detected from all over the CMS membrane by EPMA analyses when membranes were prepared with an iron containing precursor. On the contrary, accumulation of iron was observed by EMPA analyses when higher pyrolysis temperature as 1073K was applied. Figure 6c and d show TEM analysis of powder prepared under the same conditions as CMS membranes with iron additive. Iron particles were not observed in this study, but TEM-EDS confirmed the existence of iron in the sample. The hollow diffraction pattern suggested iron was in an amorphous state. These results are different from previously reported CMS membranes with inorganic additives, such as γ-alumina, silver, platinum and palladium, where these additives were dispersed as nano-particles of ca. 5-30 nm in the CMS membranes as observed by TEM[25, 27]. Iron(Ⅱ) ions and carboxylic acid group of the precursor made crosslinking, helping the homogeneous incorporation of iron[28]. We have observed changes in TG curves by mixing iron compounds as

shown in Figure 5, which suggests interaction between iron compounds and the precursors. Such interaction between iron and precursor may have prevented agglomeration and growth of metal particles at low pyrolysis temperature of 773K, and resulted in much smaller size of iron additives. Chu et al. prepared CMS membranes by mixing iron(Ⅱ) to a 6FDA-based polyimide precursor[28] They reported that applying a low pyrolysis temperature of 823K and a fast ramping rate gave the highest olefin/paraffin separation. However, the influence of iron addition was much less significant when higher pyrolysis temperature of 948K was applied. Based on the X-ray absorption near edge structure results, they suggested the pyrolysis conditions changed the iron state from Fe^{2+}, which has a strong affinity to olefins, to Fe^{3+} and Fe^{0}. The pyrolysis temperature program seems to affect not only the distribution and the size of iron compounds but also the oxidation status, which affects both the diffusion and the sorption properties of the CMS membranes.

Permeation performance of CMS membranes prepared with and without iron additive

Figure 7 shows the single gas permeance as a function of kinetic diameter of gaseous molecules through CMS membranes prepared with and without adding iron compounds to the precursor. As a comparison, CMS membranes prepared at different temperature from pure OrL precursor are also included in Figure 7a. All the membranes except OrL-973 were formed after a

single step of dip-coating, dry and pyrolysis. The OrL-973 membrane was formed after repeating the dip-coating, drying and pyrolysis cycle for three times to eliminate defects from the membrane. Permeance dropped as the size of gaseous molecules increased, showing that the molecular-sieving transport mechanism was dominant. Closed keys in Figure 7a show the results with a CMS membrane prepared at 773K using a precursor containing iron compound. The hydrogen permeance through the OrL-773 and the OrL+Fe-773 membranes were 17 $nmol \cdot m^{-2} \cdot s^{-1} \cdot Pa^{-1}$ and 13 $nmol \cdot m^{-2} \cdot s^{-1} \cdot Pa^{-1}$. The influence of iron addition was not significant on the hydrogen permeance when comparing the results obtained with OrL-773 and OrL+Fe-773 membranes. On the contrary, clear declines were observed on the permeance of larger molecules, such as oxygen, nitrogen and methane. For example the oxygen permeance decreased from 27 to 4.2 $nmol \cdot m^{-2} \cdot s^{-1} \cdot Pa^{-1}$ by incorporating iron compounds. Accordingly, the ideal selectivities were improved from the values of a CMS membrane prepared at the same temperature without iron additive. The OrL+Fe-773 membrane showed equivalent hydrogen selectivity to OrL-973 membrane, even though the pyrolysis was performed at 200 K lower temperature. For example the H_2/CH_4 and the H_2/N_2 ideal selectivities were over 500 and 200, respectively, for both membranes. On the contrary, the hydrogen permeance through the OrL+Fe-773 membrane was 132 $nmol \cdot m^{-2} \cdot s^{-1} \cdot Pa^{-1}$ as shown in Table1, which was more than 30 times larger than the permeance of the OrL-973 membrane. Defect-free membranes were not obtained when

membranes with iron additive were pyrolyzed at 873K, or membranes were prepared with 4 times more amount of iron additive. Higher pyrolysis temperature and higher iron loading may cause agglomeration of iron compound, resulting in a defect formation.

Similar influence of iron additive was observed with BP precursor as shown in Figure 7b. Results of 5 membranes are shown in the figure. Addition of iron additive did not affect hydrogen permeance but reduced permeance of nitrogen and methane. Low pyrolysis temperature and iron additives may affect the affinity of CMS membranes with toluene or other molecules. Further study is required to evaluate the properties of CMS membranes in application conditions.

Figure 8 compares the results obtained in this study with other studies. A clear trade-off between permeance and selectivity can be observed with CMS membranes prepared without iron additives but with different pyrolysis temperature. For example, the hydrogen selectivity increased with increasing the pyrolysis temperature from 673K to 973K. In contrast, the hydrogen permeance decreased from ca. 200 $nmol \cdot m^{-2} \cdot s^{-1} \cdot Pa^{-1}$ to 3.7 $nmol \cdot m^{-2} \cdot s^{-1} \cdot Pa^{-1}$ when the pyrolysis temperature was increased from 773 K to 973K. CMS membranes prepared with the iron compounds and under low pyrolysis temperature of 773K showed enhanced hydrogen selectivity but the hydrogen permeance was maintained. For example, the highest H_2/N_2 ideal selectivity obtained with membranes prepared at 773K changed from 64 to 290 by mixing iron

compounds to the precursor. On the contrary, the hydrogen permeance of these membranes was 140 and 130 nmol·m^{-2}·s^{-1}·Pa^{-1} for a membrane prepared without and with iron compounds, respectively and did not show significant influence from the iron additives.

Assumed micro-pore structure

The size of ultra-micro-pores in the CMS membranes was estimated by using the normalized Knudsen-based permeance (NKP) model. This model gives an idea of the size of penetrated ultra-micro-pores in the membrane from experimentally obtained permeance of different gas molecules [34]. According to the NKP model, a normalized permeance, f_{NKP}, and the pore size, d_p, have a relation as in the following equation

$$f_{NKP} = \frac{P_i}{P_{He}}\sqrt{\frac{M_i}{M_{He}}} \approx \left(\frac{1-(d_i/d_p)}{1-(d_{He}/d_p)}\right)^3$$

, where M_i is the molecular weight of component i and d_i is the kinetic diameter of gaseous molecule. This model does not consider the interaction between a molecule and the pore wall. However, Lee et al. showed the NKP model can describe the pore size of zeolite membranes using single gas permeance values [35]. They also applied this model to estimate the pore size of silica membranes[35, 36]. The application of the NKP model to CMS membranes needs consideration as CMS membranes have slit-like pores and show strong affinity to certain gaseous molecules. The model is used here to compare membranes prepared under different

conditions. Following the equation, permeance of various gases was normalized by dividing the values with helium permeance and shown in Figure 9. As the model does not consider surface diffusion, CO_2 permeance values that may contain strong influence of adsorption were not used. Even though, the helium permeance was about 30 times larger with OrL+Fe-773 membrane compared to the value obtained with OrL-973 membrane, the normalized permeances of these membranes were overlapped, suggesting the pore size is similar. Normalized permeances obtained with OrL-773 membrane fit best by assuming the pore size as 0.51 nm. On the contrary, both results of OrL-973 and OrL+Fe-773 membranes fit better by assuming the pore size as 0.41 nm.

Addition of small amount of iron compounds to the precursor resulted in improving the hydrogen selectivity without giving significant influence to the hydrogen permeance. From TEM-EDS, the size of iron compounds after pyrolysis seemed to be very small. Even though further study is required to understand the pore-structure of CMS membranes, assuming a formation of neck-structured pore by additives as shown in Figure 10 is one way to explain these results. The pores in CMS membranes after low pyrolysis temperature as 573K are rather loose (Fig. 10 a). By applying higher pyrolysis temperature, the pores in CMS membranes shrink. That results in higher hydrogen selectivity but lower hydrogen permeance (Fig.10 b). On the contrary, the addition of a small amount of iron compounds and the use of low pyrolysis

temperature distributes additives in the pores, forming neck-like structure that improves the hydrogen selectivity. As the main pore structure is kept loose, the hydrogen permeance did not decrease much (Fig. 10c). Similar results were obtained by Suda et al.[26] and by Chu et al.[28]. Suda et al. mixed ferrocene ($Fe(C_5H_5)_2$) to PDMA-ODA polyimide and prepared CMS films. They found addition of 5 and 10wt% of iron decreased larger gases, such as CO_2, O_2, CO and N_2 greatly but permeance of H_2 and He were almost the same. Chu et al. mixed between 1.1 and 3.2 wt% of Fe(Ⅱ) acetylacetonates to a 6FDA-based polyimide and prepared CMS membranes. One of the reasons for incorporating Fe(Ⅱ) was its high C_2H_4/C_2H_6 selectivity. The resulting membranes showed enhanced olefin selectivity. However, the enhancement was larger than what was expected from the sorption enhancement caused by incorporated Fe(Ⅱ). They proposed that the iron complex narrowed the pore size of ultra-micro pores, which is similar to what is observed in our study by mixing Fe(Ⅲ) to organosolve lignin.

Aging of the CMS membranes

Figure 11 shows the change of permeance after keeping the membranes in a room at ambient conditions. The first points were measured the day after of the CMS membrane preparation. Hydrogen permeance through CMS membranes formed from pure OrL precursor decreased with the time of exposure to the air ("□" keys in the figure). After about 400 days, the hydrogen

permeance became about half of the fresh membrane and seemed to be reaching for a stable value. Reduction of hydrogen permeance was also observed when a CMS membrane was prepared from OrL precursor with iron additive ("■" keys in the figure). The reduction rates were larger for CO_2 and N_2. Xu et al. [37] reported that besides the chemisorption of oxygen to the edges of pores, physical aging also contributed to the decrease of permeance through CMS membranes with time. Menendez et al. reported that the air-aged CMS membranes got irreversible chemisorption of oxygen and can be only partially regenerated by heat treatment[38]. In our study also, the hydrogen permeance did not improve even after treating the membrane at 408K in vacuum for several hours. CMS membranes prepared with iron additives showed similar decline but the reduction rates were larger compared to those values obtained with CMS membranes prepared from pure OrL precursor. Iron state in the CMS membrane is unknown and requires further investigation, however, oxidation of iron or other change may enhance the partial densification.

Conclusion

CMS membranes were prepared by a single process of dip-coating, drying and pyrolysis on porous alumina tubes. OrL was successfully used as a precursor for a CMS membrane formation. Adding a small amount of iron(Ⅲ) acetate basic to OrL and BP precursors

improved the hydrogen selectivity of the resulting CMS membranes without giving significant change of the hydrogen permeance compared to CMS membranes prepared under the same pyrolysis temperature. Low pyrolysis temperature as 773K prevented the agglomeration of iron additives. The rather loose pore network formed at 773K in the CMS membranes may be partially densified by the iron additives. Combination of low pyrolysis temperature and additives may be one way to improve both the hydrogen permeance and selectivity.

Acknowledgements

We acknowledge the financial support from Tonen General Research Fund and MEXT/JSPS KAKENHI Grant number C17K06893.

References

(1) Rogelj, J.; den Elzen, M.; Höhne, N.; Fransen, T.; Fekete, H.; Winkler, H.; Schaeffer, R.; Sha, F.; Riahi, K.; Meinshausen, M., Paris Agreement climate proposals need a boost to keep warming well below 2 °C. *Nature* **2016,** 534, 631.
(2) Dutta, S., A review on production, storage of hydrogen and its utilization as an energy resource. *Journal of Industrial and Engineering Chemistry* **2014,** 20, (4), 1148-1156.
(3) Gretz, J.; Baselt, J. P.; Ullmann, O.; Wendt, H., The 100 MW euro-Quebec hydro-hydrogen pilot project. *International Journal of Hydrogen Energy* **1990,** 15, (6), 419-424.
(4) Okada, Y.; Shimura, M. In *Development of large-scale H2 storage and transportation technology with Liquid Organic Hydrogen Carrier (LOHC)* **2013,** *Proceedings of The 21st Joint GCC-Japan Environment Symposium*, Doha, Qatar.
(5) Saito, Y.; Okada, Y., Topic: Organic Hydride for Hydrogen Energy Carrier. In *Energy Technology Roadmaps of Japan: Future Energy Systems Based on Feasible Technologies Beyond 2030*, Kato, Y.; Koyama, M.; Fukushima, Y.; Nakagaki, T., Eds. Springer Japan: Tokyo,

2016; pp 459-462.
(6) Oda, K.; Akamatsu, K.; Sugawara, T.; Kikuchi, R.; Segawa, A.; Nakao, S.-i., Dehydrogenation of Methylcyclohexane To Produce High-Purity Hydrogen Using Membrane Reactors with Amorphous Silica Membranes. *Industrial & Engineering Chemistry Research* **2010,** 49, (22), 11287-11293.
(7) Nakayama, J.; Misono, H.; Sakamoto, J.; Kasai, N.; Shibutani, T.; Miyake, A., Simulation-based safety investigation of a hydrogen fueling station with an on-site hydrogen production system involving methylcyclohexane. *International Journal of Hydrogen Energy* **2017,** 42, (15), 10636-10644.
(8) Haraya, K.; Yoshimune, M., Evaluation of Membrane Separation Processes for Recovery and Purification of Hydrogen Derived from Dehydrogenation of Methylcyclohexane. *Journal of the Japan Pertoleum Institute* **2016,** 59, (6), 299-306.
(9) Li, G.; Niimi, T.; Kanezashi, M.; Yoshioka, T.; Tsuru, T., Equilibrium shift of methylcyclohexane dehydrogenation in a thermally stable organosilica membrane reactor for high-purity hydrogen production. *International Journal of Hydrogen Energy* **2013,** 38, (35), 15302-15306.
(10) Meng, L.; Yu, X.; Niimi, T.; Nagasawa, H.; Kanezashi, M.; Yoshioka, T.; Tsuru, T., Methylcyclohexane dehydrogenation for hydrogen production via a bimodal catalytic membrane reactor. *AIChE Journal* **2015,** 61, (5), 1628-1638.
(11) Zhang, X.-L.; Akamatsu, K.; Nakao, S.-i., Hydrogen Separation in Hydrogen–Methylcyclohexane–Toluene Gaseous Mixtures through Triphenylmethoxysilane-Derived Silica Membranes Prepared by Chemical Vapor Deposition. *Industrial & Engineering Chemistry Research* **2016,** 55, (18), 5395-5402.
(12) Howard, B. H.; Killmeyer, R. P.; Rothenberger, K. S.; Cugini, A. V.; Morreale, B. D.; Enick, R. M.; Bustamante, F., Hydrogen permeance of palladium–copper alloy membranes over a wide range of temperatures and pressures. *Journal of Membrane Science* **2004,** 241, (2), 207-218.
(13) Kumakiri, I.; Qiu, L.; Liu, B.; Tanaka, K.; Kita, H.; Saito, T.; Nishida, R., Application of MFI Zeolite Membrane Prepared with Fluoride Ions to Hydrogen/Toluene Separation. *Journal of Chemical Engineering of Japan* **2016,** 49, (8), 753-755.
(14) Briceño, K.; Iulianelli, A.; Montané, D.; Garcia-Valls, R.; Basile, A., Carbon molecular sieve membranes supported on non-modified ceramic tubes for hydrogen separation in membrane reactors. *International Journal of Hydrogen Energy* **2012,** 37, (18), 13536-13544.
(15) Yoshimune, M.; Haraya, K., Ultrapure Hydrogen Purification Derived from Organic Chemical Hydrides using Carbon Membranes for Hydrogen Stations. *MEMBRANE* **2016,** 41, (3), 96-101.
(16) Niimi, T.; Nagasawa, H.; Kanezashi, M.; Yoshioka, T.; Ito, K.; Tsuru, T., Preparation of

BTESE-derived organosilica membranes for catalytic membrane reactors of methylcyclohexane dehydrogenation. *Journal of Membrane Science* **2014,** 455, 375-383.
(17) Yoshimune, M.; Haraya, K., Flexible carbon hollow fiber membranes derived from sulfonated poly(phenylene oxide). *Separation and Purification Technology* **2010,** 75, (2), 193-197.
(18) He, X.; Hägg, M.-B., Hollow fiber carbon membranes: Investigations for CO2 capture. *Journal of Membrane Science* **2011,** 378, (1), 1-9.
(19) Rungta, M.; Wenz, G. B.; Zhang, C.; Xu, L.; Qiu, W.; Adams, J. S.; Koros, W. J., Carbon molecular sieve structure development and membrane performance relationships. *Carbon* **2017,** 115, (Supplement C), 237-248.
(20) Shiflett, M. B.; Foley, H. C., On the preparation of supported nanoporous carbon membranes. *Journal of Membrane Science* **2000,** 179, (1–2), 275-282.
(21) Song, C.; Wang, T.; Wang, X.; Qiu, J.; Cao, Y., Preparation and gas separation properties of poly(furfuryl alcohol)-based C/CMS composite membranes. *Separation and Purification Technology* **2008,** 58, (3), 412-418.
(22) Wang, C.; Ling, L.; Huang, Y.; Yao, Y.; Song, Q., Decoration of porous ceramic substrate with pencil for enhanced gas separation performance of carbon membrane. *Carbon* **2015,** 84, 151-159.
(23) Saufi, S. M.; Ismail, A. F., Fabrication of carbon membranes for gas separation—a review. *Carbon* **2004,** 42, (2), 241-259.
(24) Lie, J. A.; He, X.; Kumakiri, I.; Kita, H.; Hagg, M.-B., Carbon based Membranes. *H2 production and separation/purification, Senior Commissioning Editor-Books* **2017**, 401-427.
(25) Yoda, S.; Hasegawa, A.; Suda, H.; Uchimaru, Y.; Haraya, K.; Tsuji, T.; Otake, K., Preparation of a Platinum and Palladium/Polyimide Nanocomposite Film as a Precursor of Metal-Doped Carbon Molecular Sieve Membrane via Supercritical Impregnation. *Chemistry of Materials* **2004,** 16, (12), 2363-2368.
(26) Suda, H.; Yoda, S.; Hasegawa, A.; Tsuji, T.; Otake, K.; Haraya, K., Gas permeation properties of carbon molecular sieve membranes dispersed with palladium nano particles via supercritical CO2 impregnation. *Desalination* **2006,** 193, (1), 211-214.
(27) Teixeira, M.; Campo, M.; Tanaka, D. A.; Tanco, M. A.; Magen, C.; Mendes, A., Carbon–Al2O3–Ag composite molecular sieve membranes for gas separation. *Chemical Engineering Research and Design* **2012,** 90, (12), 2338-2345.
(28) Chu, Y.-H.; Yancey, D.; Xu, L.; Martinez, M.; Brayden, M.; Koros, W., Iron-containing carbon molecular sieve membranes for advanced olefin/paraffin separations. *Journal of Membrane Science* **2018,** 548, 609-620.
(29) Hirota, Y.; Ishikado, A.; Uchida, Y.; Egashira, Y.; Nishiyama, N., Pore size control of

microporous carbon membranes by post-synthesis activation and their use in a membrane reactor for dehydrogenation of methylcyclohexane. *Journal of Membrane Science* **2013,** 440, 134-139.

(30) http://www.awi.co.jp/bp/e/pg/01.html

(31) Ismail, A. F.; David, L. I. B., A review on the latest development of carbon membranes for gas separation. *Journal of Membrane Science* **2001,** 193, (1), 1-18.

(32) Zdravkov, B.; Čermák, J.; Šefara, M.; Janků, J., Pore classification in the characterization of porous materials: A perspective. *Open Chemistry* **2007,** 5, (2), 385-395.

(33) Jewur, S. S.; Kuriacose, J. C., Studies on the thermal decomposition of ferric acetate. *Thermochimica Acta* **1977,** 19, (2), 195-200.

(34) Yoshioka, T.; Kanezashi, M.; Tsuru, T., Micropore size estimation on gas separation membranes: A study in experimental and molecular dynamics. *AIChE Journal* **2013,** 59, (6), 2179-2194.

(35) Lee, H. R.; Kanezashi, M.; Shimomura, Y.; Yoshioka, T.; Tsuru, T., Evaluation and fabrication of pore‐size‐tuned silica membranes with tetraethoxydimethyl disiloxane for gas separation. *AIChE Journal* **2011,** 57, (10), 2755-2765.

(36) Kanezashi, M.; Kawano, M.; Yoshioka, T.; Tsuru, T., Organic–Inorganic Hybrid Silica Membranes with Controlled Silica Network Size for Propylene/Propane Separation. *Industrial & Engineering Chemistry Research* **2012,** 51, (2), 944-953.

(37) Xu, L.; Rungta, M.; Hessler, J.; Qiu, W.; Brayden, M.; Martinez, M.; Barbay, G.; Koros, W. J., Physical aging in carbon molecular sieve membranes. *Carbon* **2014,** 80, (Supplement C), 155-166.

(38) Menendez, I.; Fuertes, A. B., Aging of carbon membranes under different environments. *Carbon* **2001,** 39, (5), 733-740.

Table and Figure Captions

Table 1 Gas permeance and ideal selectivity of CMS membranes calcined at different temperatures (the thickness of the CMS membranes were ca. 1 micrometer)

Figure 1 Structure of OrL (Reproduced with permission from Sigma-Aldrich Co. LLC (sigma-aldrich.com))

Figure 2 Pyrolysis temperature program

Figure 3 Schematic illustration of a permeation test rig

Figure 4 Influence of pyrolysis temperature on the CMS membranes prepared with pure OrL precursor (a) permeance as a function of pyrolysis temperature, ○: He, □; H_2, ◊: CO_2, Δ:O_2, ⊿: N_2, ∇:CH_4, +: CF_4, b) ideal selectivity as a function of pyrolysis temperature, dotted lines in the figure are interpolation)

Figure 5 Weight change of precursors as a function of temperature measured at heating rate of 5K/min in nitrogen (a) OrL, b) BP, solid lines: without additive, dashed lines: with iron(Ⅲ) acetate basic)

Figure 6 a) Cross-sectional view of a CMS membrane formed after pyrolysis at 773K using a precursor containing iron, b) carbon distribution in the membrane measured by EPMA, c) TEM

image of carbon sample prepared at 773K with the same precursor as a), d) element analysis of c) by TEM-EDS

Figure 7 Single gas permeance as a function of kinetic diameter of gas molecules (a) OrL precursor, b) BP precursor, open keys are without additives, closed keys are with iron compounds) (measurements were performed at 308K and feed pressure 1.1 bar, by a fixed volume pressure-increase measurement)

Figure 8 Comparison of H_2/N_2 ideal selectivity as a function of hydrogen permeance measured with composite CMS membranes (x:[20], ◩:[21], +:[14], ◪:[22], ○:organo-solve liginin coated membrane (without pyrolysis), Δ: CMS membranes prepared at 673K, ○: CMS membranes prepared at 773K, ◊: CMS membranes prepared at 873K , ▷: CMS membranes prepared at 973K and ●: CMS membranes prepaed from iron containing precursor and at 773K)

Figure9 Normalized permeance based on the NKP model as a function of kinetic diameter of gas molecules (lines in the figure were calculated using the equation assuming the pore size as indicated in the figure)

Figure 10 Images of micro-pores in CMS membranes prepared under different conditions (a) after low temperature pyrolysis, b)after high temperature pyrolysis, c) after low temperature pyrolysis with additives)

Figure 11 Influence of aging under ambient conditions on the permeance through CMS membranes (open keys: CMS membrane prepared from pure OrL precursor, closed keys: CMS membrane prepared from OrL + Fe precursor)

Table 1 Gas permeance and ideal selectivity of CMS membranes pyrolized at different temperatures (the thickness of the CMS membranes were ca. 1 micrometer)

Membrane No.*	Permeance, P(i) [10^{-9} mol $m^{-2}s^{-1}Pa^{-1}$]**		Ideal selectivity [-]				
	$P(H_2)$	$P(CO_2)$	H_2/CH_4	H_2/N_2	H_2/O_2	CO_2/N_2	CO_2/CH_4
OrL-none-1	25.1	5.62	2.6	3.3	3.8	0.75	0.58
OrL-673-3	47.8	36.7	8.0	9.1	4.7	7.0	6.2
OrL-773-1	169	29.5	54	32	6.3	5.6	9.5
OrL-773-3	124	80.9	54	32	6.1	21	35
OrL-873-1	16.9	1.67	138	142	4	14	14
OrL-873-3	12.3	3.22	540	130	15	35	140
OrL-973-3	3.65	0.36	630	230	29	22	63
OrL-1073-3	0.49	0.31	1.8	3.2	2.1	2.0	1.1
OrL+ Fe-773-1	132	16.7	584	293	32	37	74

* Number shows "precursor - pyrolysis temperature in K - number of coating and pyrolysis process"

** 1GPU = $1x10^{-6}$ cm^3 STP cm^{-2} s^{-1} $cmHg^{-1}$ = $3.35x10^{-10}$ mol $m^{-2}s^{-1}Pa^{-1}$

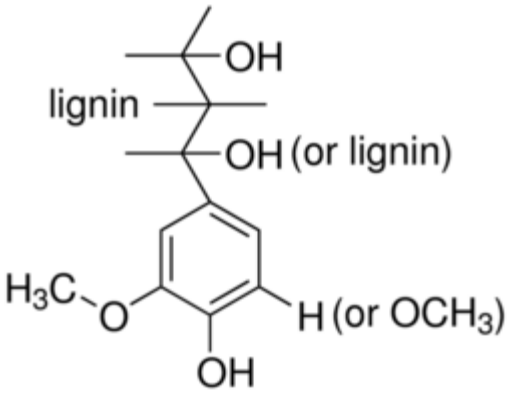

Figure 1 Structure of OrL (Reproduced with permission from Sigma-Aldrich Co. LLC (sigma-aldrich.com))

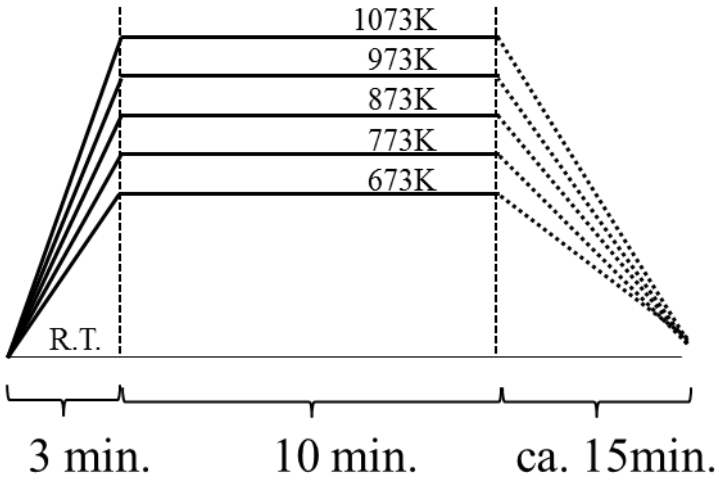

Figure 2 Pyrolysis temperature program

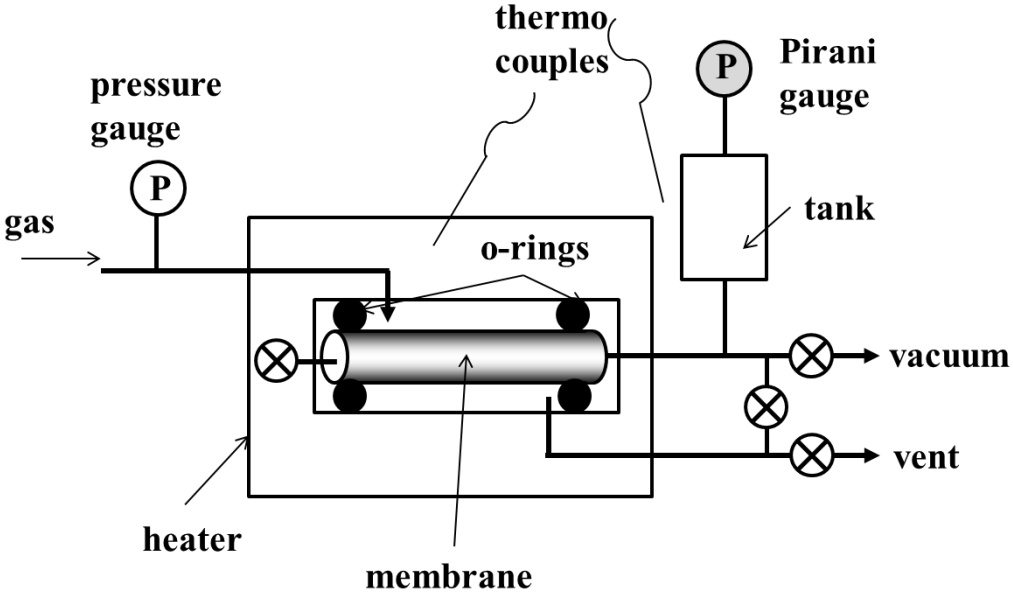

Figure 3 Schematic illustration of a permeation test rig

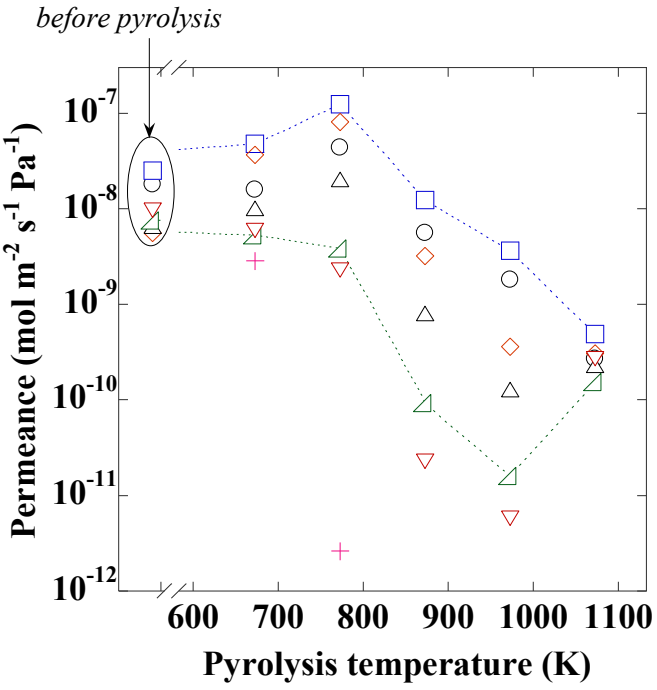

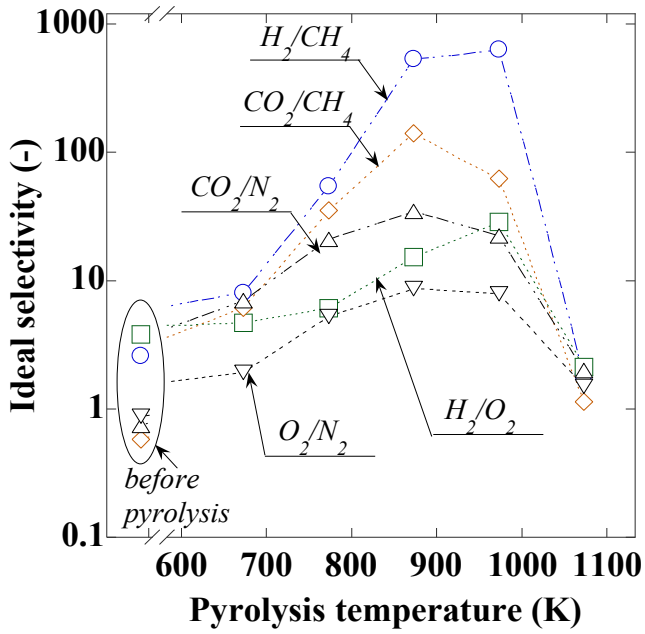

Figure 4 Influence of pyrolysis temperature on the CMS membranes prepared with pure OrL precursor (a) permeance as a function of pyrolysis temperature, ○: He, □; H_2, ◊: CO_2, Δ:O_2, ⊿:

N_2, ∇:CH_4, +: CF_4, b) ideal selectivity as a function of pyrolysis temperature, dotted lines in the figure are interpolation)

a)

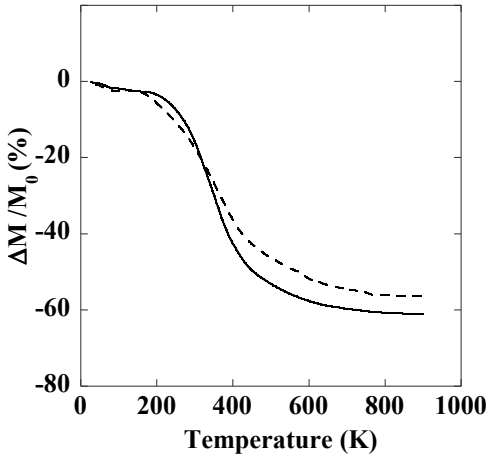

b)

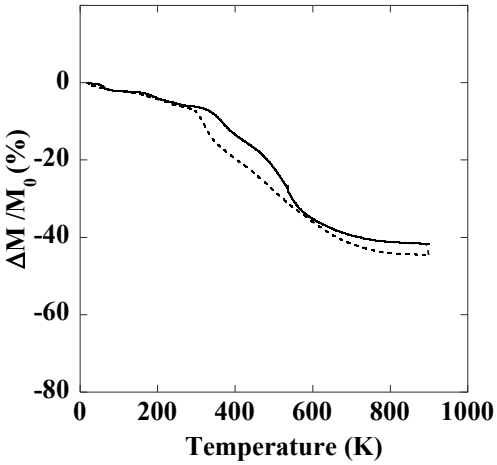

Figure 5 Weight change of precursors as a function of temperature measured at heating rate of 5K/min in nitrogen (a) OrL, b) BP, solid lines: without additive, dashed lines: with iron(Ⅲ) acetate basic)

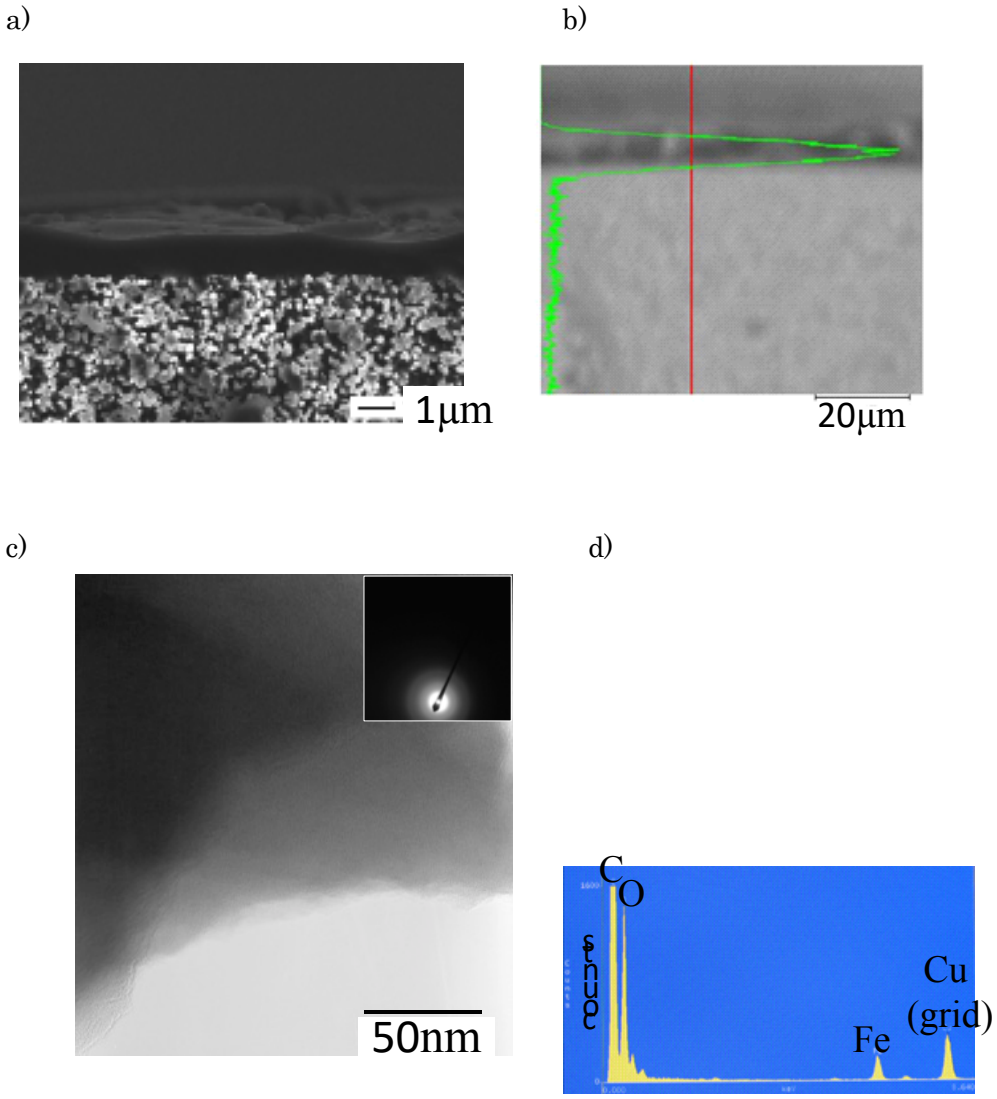

Figure 6 a) Cross-sectional view of a CMS membrane formed after pyrolysis at 773K using a precursor containing iron, b) carbon distribution in the membrane measured by EPMA, c) TEM image of carbon sample prepared at 773K with the same precursor as a), d) element analysis of c) by TEM-EDS

a)

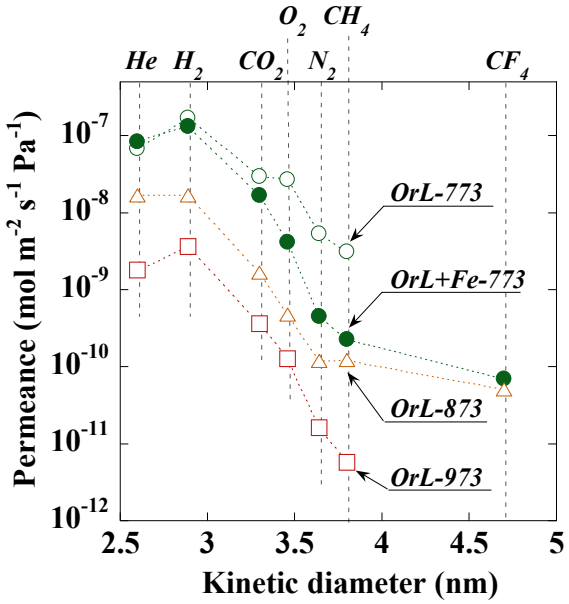

b)

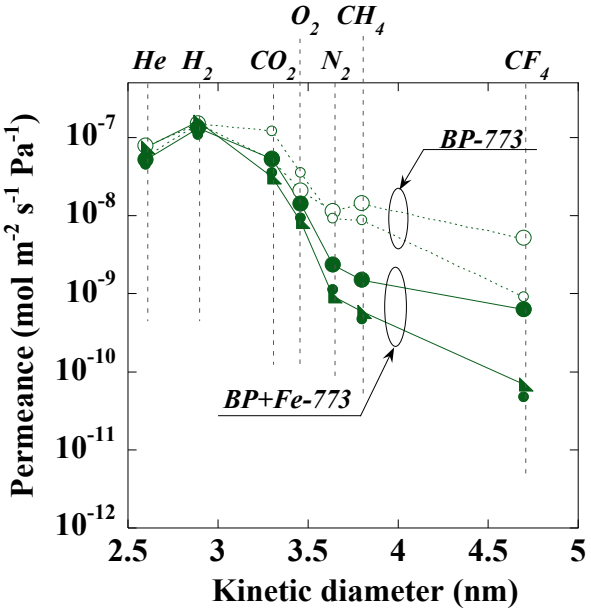

Figure 7 Single gas permeance as a function of kinetic diameter of gas molecules (a) OrL precursor, b) BP precursor, open keys are without additives, closed keys are with iron compounds) (measurements were performed at 308K and feed pressure 1.1 bar, by a fixed volume pressure-increase measurement)

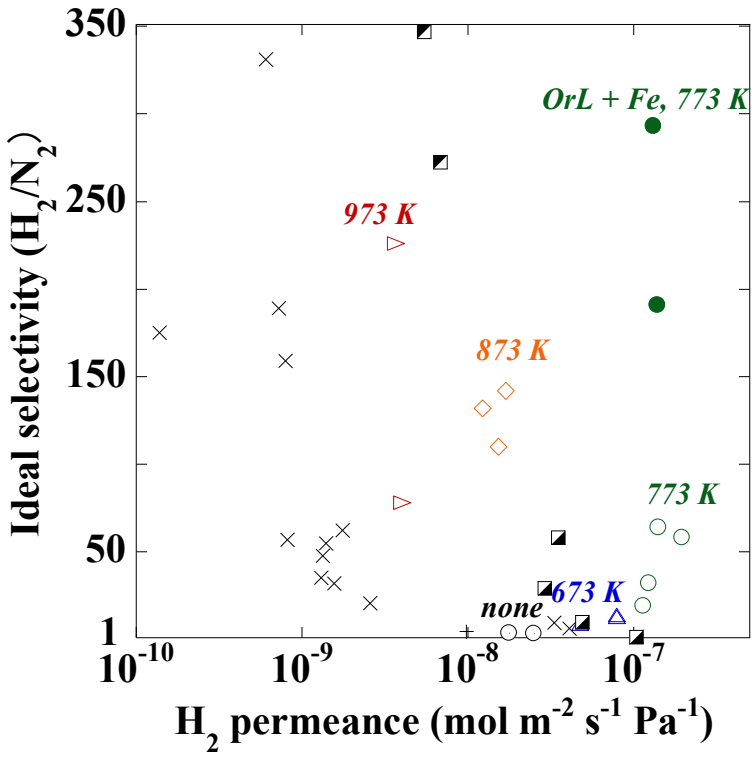

Figure 8 Comparison of H_2/N_2 ideal selectivity as a function of hydrogen permeance measured with composite CMS membranes (x:[20], ◩:[21], +:[14], ◪:[22], ○:organo-solve liginin coated membrane (without pyrolysis), Δ: CMS membranes prepared at 673K, ○: CMS membranes prepared at 773K, ◊: CMS membranes prepared at 873K , ▷: CMS membranes prepared at 973K and ●: CMS membranes prepaed from iron containing precursor and at 773K)

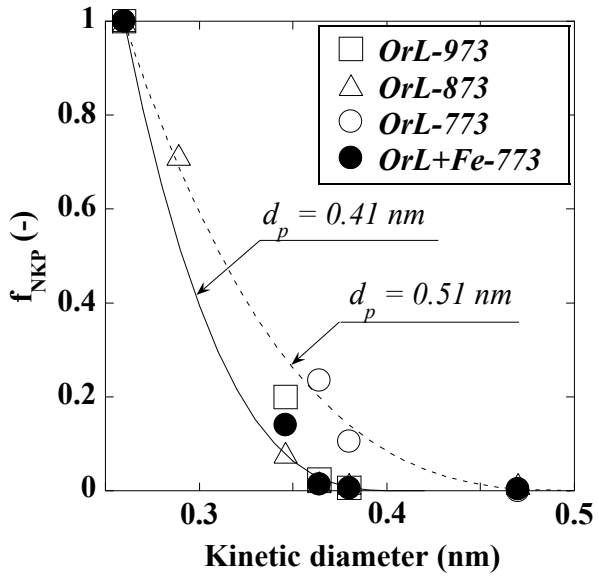

Figure 9 Normalized permeance based on the NKP model as a function of kinetic diameter of gas molecules (lines in the figure were calculated using the NKP model assuming the pore size as indicated in the figure)

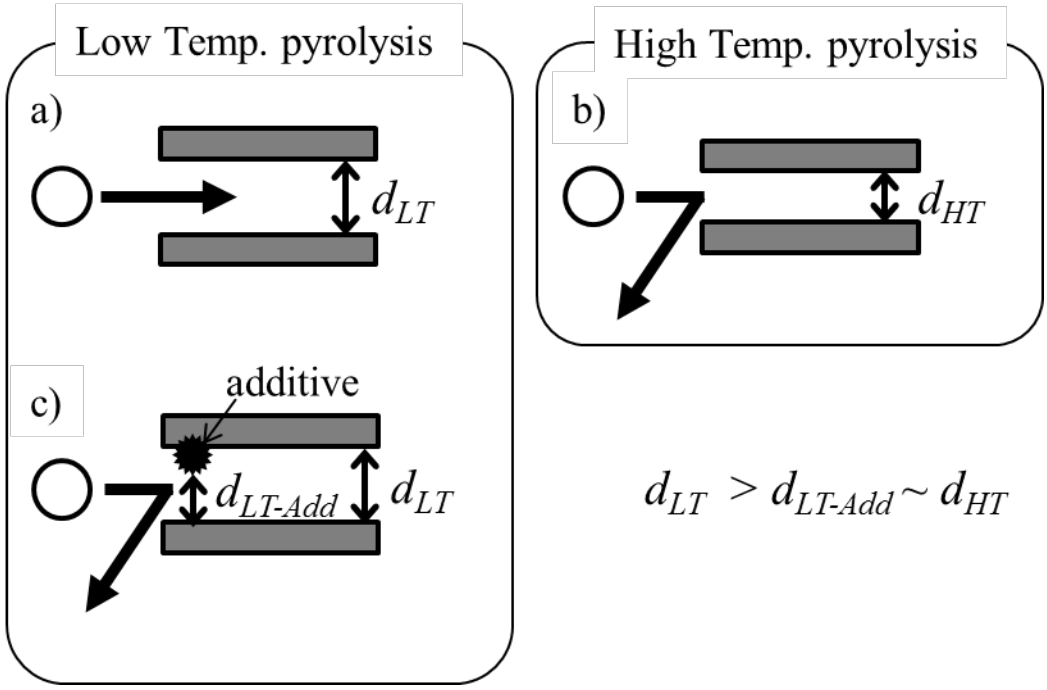

Figure 10 Images of micro-pores in CMS membranes prepared under different conditions (a) after low temperature pyrolysis, b)after high temperature pyrolysis, c) after low temperature pyrolysis with additives)

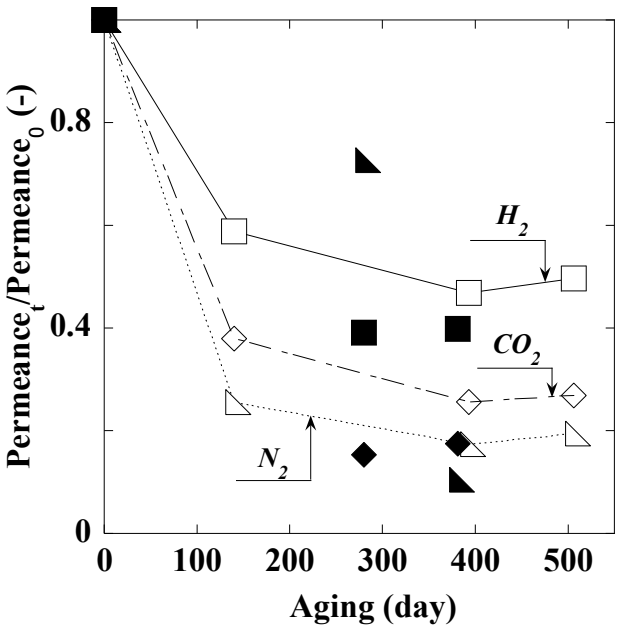

Figure 11 Influence of aging under ambient conditions on the permeance through CMS membranes (open keys: CMS membrane prepared from pure OrL precursor, closed keys: CMS membrane prepared from OrL + Fe precursor)

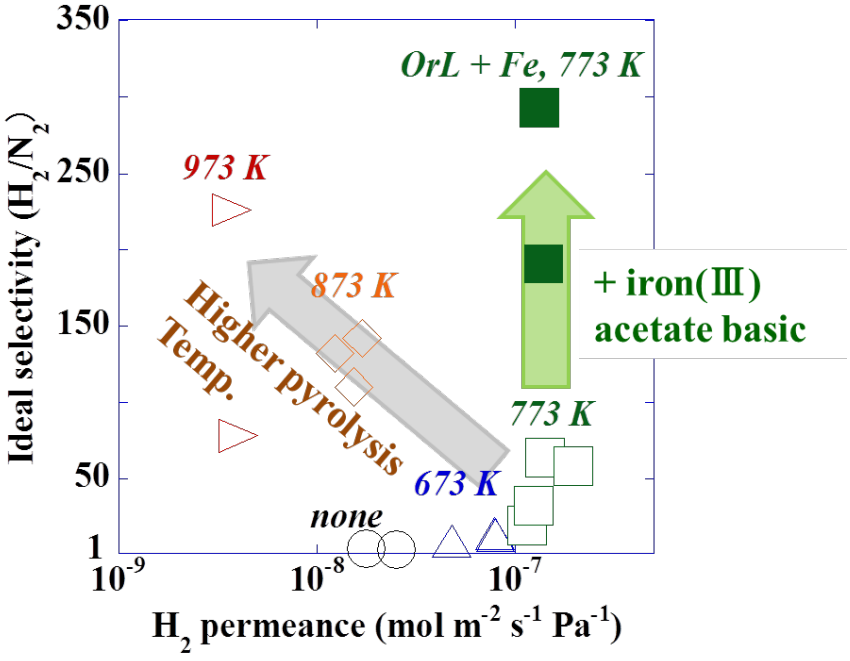

Graphical abstract